PRESENT-DAY MASS BALANCE OF MARTIAN ICY OUTLIERS. J. Bapst[1,2,*], S. Byrne[1], and A. J. Brown[3] [1]Lunar and Planetary Laboratory, University of Arizona, Tucson, AZ, 85721. [2]Dept. of Earth and Space Sciences, University of Washington, Seattle, WA, 98195. [3]SETI Institute, 189 N. Bernardo Ave, Mountain View, CA. [*]jnbapst@lpl.arizona.edu

Introduction: The northern plains of Mars contain at least 11 craters poleward of 70° that host exposed water ice mounds [1]. These circumpolar ice mounds represent the warmest perennial surface ice on Mars and are therefore important in understanding the recent and present climate of Mars.

The smallest of these mounds is found in Louth crater, a 36 km diameter crater located at 70°N, 103°E and hosts an ice mound ~10 km diameter, and up to ~250 m thick. The largest of these mounds is found in 83 km diameter Korolev crater (73°N, 164°E) which hosts a ~60 km diameter mound. In certain areas this deposit approaches nearly 2 km in thickness (both shown in Fig. 1).

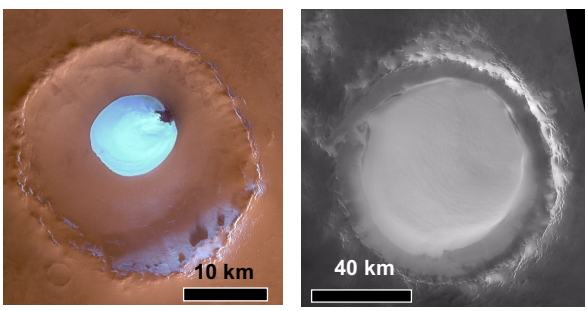

Figure 1. Louth (left) and Korolev (right) craters and their ice mounds. North is up in both images. HRSC_234192 (left) and H5726_0001_ND3 (right).

Previous work, analyzing repeat high-resolution images of the Louth ice mound, documented removal and replacement of ice near the mound boundary [2]. Although a secular trend was not clear in this analysis, it has been suggested that this ice mound is in a current state of ablation [3]. Our other study case, Korolev, is expected to be more stable, being at a slightly higher latitude.

Here, using a set of 1-D models, we estimate the mass balance of both Korolev and Louth crater ice mounds for a range of atmospheric water abundances and surface albedo. Unlike the Louth ice mound, the Korolev case is easily resolved by the resolution of Mar Global Surveyor Thermal Emission Spectrometer (TES; [4]). TES Temperatures are used to constrain our model. Because TES cannot resolve Louth, we use the thermal properties derived from Korolev temperatures.

Methods: Mass balance is calculated by coupling thermal model output (i.e., temperatures) to a boundary-layer model that handles water mixing in the atmosphere and water ice deposition/ablation at the surface.

Thermal Model: A 1-D semi-implicit thermal model is modified to produce annual temperatures representative of the ice mounds in Louth and Korolev craters. Using a single layer model, we constrain the thermal inertia (TI) and albedo using TES target temperatures. We calculate a reduced chi-squared statistic in order to identify best fit parameters, i.e., TI and albedo. We calculate fitting parameters for three Korolev temperature sets: AM, PM and AM+PM (Fig. 2).

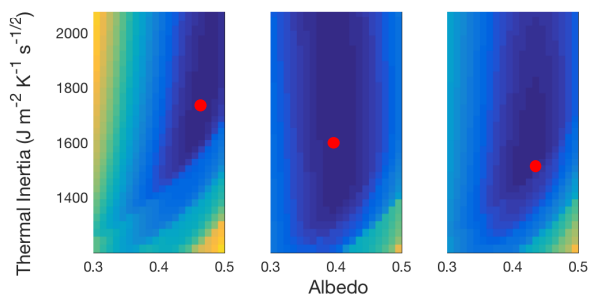

Figure 2. Reduced χ^2 values for modeled Korolev ice mound temperatures against TES data. Cooler colors represent lower values, i.e. better fits. Fits from left to right: AM, PM, and AM+PM. Best-fit TI and albedo (α) are marked by a red circle. Best fit models for AM: TI=1720, α=0.46, χ^2=17.3; PM: TI=1610, α=0.40, χ^2=141; AM+PM: TI=1540, α=0.42, χ^2=75.6; TI in units of J m^{-2} K^{-1} s$^{-1/2}$.

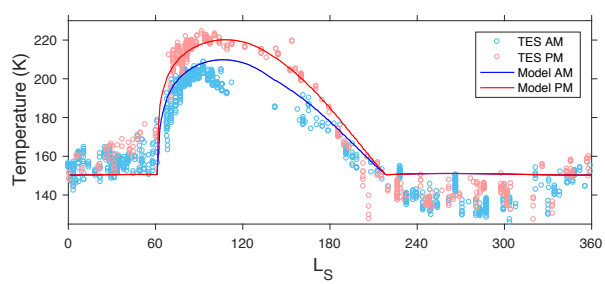

Figure 3. Annual AM and PM temperatures for modeled Korolev ice mound plotted over TES data. (TI = 1720 J m^{-2} K^{-1} s$^{-1/2}$, α=0.40)

We use the best-fit TI from our AM case and our best fit albedo from the PM case. These are 1720 J m^{-2} K^{-1} s$^{-1/2}$ and 0.40, respectively (Fig. 3).

Water Transport Model: We are developing a 1-D diffusion model that simulates boundary-layer water mixing and allows for water ice deposition/removal. The model is divided into two distinct zones: an upper turbulent layer that is assigned a relatively large eddy diffusivity to simulate convective mixing, and a more shallow, near-surface laminar layer where vapor

transport is governed by molecular diffusion. Our model extends from the surface to 6 km altitude.

In the upper zone, we apply a model of eddy diffusion after [5,6]. We use two different wind speeds that fall within the range of observed values (~0-10 m/s; [7]). Surface roughness is required to calculate mixing rates. We adopt a value of 0.1 cm which is used by [8] for martian ice sheets. Eddy diffusivity increases with height until the logarithmic wind profile height [5], then eddy diffusivity remains constant (Table 1).

The laminar zone thickness d, is estimated after [8]:

$$d=30\nu/u_*$$

Where ν is the kinematic viscosity of the atmosphere and u_* is the friction velocity. The diffusivity of the lower layer is based on laboratory experiments of water vapor diffusion under Mars conditions (~0.002 m^2/s; [9]). The lower boundary is controlled by the deposition and sublimation of water ice through the laminar layer.

Wind Speed at 1.6 m height (m/s)	1.0	5.0
Friction Velocity, u_* (m/s)	0.339	1.69
Laminar Layer Thickness, d (m)	0.039	0.0078
Logarithmic Wind Profile Height (m)	499	2540
Upper Layer Eddy Diffusivity (m^2/s)	67.7	1690

Table 1. Atmospheric model parameters used in this study.

The upper boundary is prescribed using 6 km altitude water vapor densities from the Laboratoire de Météorologie Dynamique Mars Climate Database (MCD) [10]. Data were acquired in 20° L_S increments. Vapor abundance is not well constrained in the lower martian atmosphere that we are specifically modeling. Therefore, we vary values at the top boundary (from MCD) by a simple factor to explore atmospheres with different water vapor concentrations.

Results: Mass balance is calculated for the Korolev ice mound using a range of albedo via our best-fit models and a range of vapor densities after MCD (Fig. 4). Results support the mound being close to net zero mass balance for unmodified MCD humidity. Annual accumulation/ablation rates are in the range of ±100 µm of water ice per Mars year (assuming ρ_{water}=1000 kg m^{-3}) for MCD factors <2.

We estimate mass balance for the Louth ice mound over a wider range of albedos as TES data do not constrain this value (Fig. 5). However, the mass balance estimates are not very different from Korolev, i.e., near equilibrium. The case with the highest ablation at Louth, u=5 m/s, α=0.40, and MCD factor of 0.1, shows 180 µm of ablation per Mars year. Results suggest mixing rate (i.e., wind speed) has a small effect on the equilibrium albedo/water abundance parameters.

Discussion: Our coupled thermal and water mixing models predict small net mass balance values for Louth and Korolev ice mounds. Our largest annual balance values, in the u=5 m/s case, are around ±200 µm per Mars year. Our atmospheric mixing model is omitting a potentially important process, free convection. Free convection will increase mixing rates for our low wind speed cases but will affect only ablation [11].

Future atmospheric modeling will expore lateral mixing between air over non-ice covered surfaces, and will refine our mass balance estimates. This will be especially important for Louth due to its size.

Finally, we'll use our model to analyze the seasonal timing of deposition versus ablation (e.g., "mode flips") that occur throughout the year on the north polar residual cap [12]. With repeat near-IR imaging we can detect mode flips for these regions and further constrain our models of ice deposition/ablation [14].

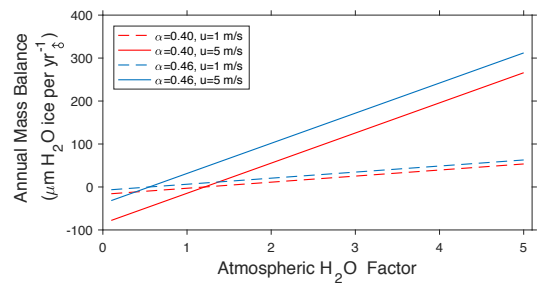

Figure 4. Annual mass balance of modeled Korolev water ice mound for range of atmospheric water abundance (factor relative to MCD value). We model 4 different cases: varying albedo between 0.40 and 0.46 and wind speed between 1 and 5 m/s.

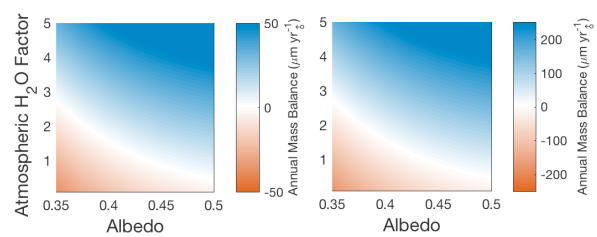

Figure 5. Louth ice mound annual mass balance for range of albedos, atmospheric water abundance, and wind speed; (left) 1 m/s, (right) 5 m/s.

References: **[1]** Conway, S. J. *et al.* (2012) *Icarus*, *220*, 174–193. **[2]** Bapst, J. and S. Byrne (2015) *LPSC 46, #*2772. **[3]** Brown, A. *et al.* (2008) *Icarus*, 196(2), 433–445. **[4]** Christensen, P. R. *et al.* (2004) *Space Sci. Rev.* 110, 85–130. **[5]** Svitek, T. and B. Murray (1990) *JGR, 95*, 1495–1510. **[6]** Zent, A. P. *et al.* (1993) *JGR* 98, 3319–3337. **[7]** Hess, S. L. *et al.* (1977) *JGR*, *82*(28), 4559–4574. **[8]** Wallace, D. and C. Sagan (1979) *Icarus*, *39*, 385–400. **[9]** Chittenden, J. D. *et al.* (2008) *Icarus*, *196*(2), 477–487. **[10]** Lewis, S. R., *et al.* (1999) *JGR,* 104, E10. **[11]** Dundas, C. M. *et al.* (2014) *JGR*., *119*, 109–127. **[12]** Brown, A. J. *et al.* (2016) *Icarus*, *277*, 401–415. **[14]** Brown, A. J. *et al.* (2017) *LPSC 48, #*2672.